

CLiMB: A Domain-Informed Novelty Detection Clustering Framework for Scientific Discovery

Lorenzo Monti *

LORENZO.MONTI@INAF.IT

Tatiana Muraveva *

TATIANA.MURAVEVA@INAF.IT

Brian Sheridan †

BRIAN.SHERIDAN@TOELT.AI

Davide Massari *

DAVIDE.MASSARI@INAF.IT

Alessia Garofalo *

ALESSIA.GAROFALO@INAF.IT

Gisella Clementini *

GISELLA.CLEMENTINI@INAF.IT

Umberto Michelucci †,‡

UMBERTO.MICHELUCCI@HSLU.CH

* *National Institute for Astrophysics, Osservatorio di Astrofisica e Scienza dello Spazio, Bologna, via Piero Gobetti 93/3, 40129, Italy*

† *TOELT LLC, Machine Learning Research and Development Department, Winterthur 8406, Zurich, Switzerland*

‡ *Computer Science Department, Lucerne University of Applied Sciences and Arts, Luzern 6002, Switzerland*

Editor: My editor

Abstract

In data-driven scientific discovery, a challenge lies in classifying well-characterized phenomena while identifying novel anomalies. Current semi-supervised clustering algorithms do not always fully address this duality, often assuming that supervisory signals are globally representative. Consequently, methods often enforce rigid constraints that suppress unanticipated patterns or require a pre-specified number of clusters, rendering them ineffective for genuine novelty detection. To bridge this gap, we introduce CLiMB (CLustering in Multiphase Boundaries), a domain-informed framework decoupling the exploitation of prior knowledge from the exploration of unknown structures. Using a sequential two-phase approach, CLiMB first anchors known clusters using constrained partitioning, and subsequently applies density-based clustering to residual data to reveal arbitrary topologies. We demonstrate this framework on RR Lyrae stars data from the *Gaia* Data Release 3. CLiMB attains an Adjusted Rand Index of 0.829 with 90% seed coverage in recovering known Milky Way substructures, drastically outperforming heuristic and constraint-based baselines, which stagnate below 0.20. Furthermore, sensitivity analysis confirms CLiMB’s superior data efficiency, showing monotonic improvement as knowledge increases. Finally, the framework successfully isolates three dynamical features (Shiva, Shakti, and the Galactic Disk) in the unlabelled field, validating its potential for scientific discovery.

Keywords: novelty detection, semi-supervised clustering, constrained clustering, density-based clustering, domain knowledge integration

1 Introduction

In modern scientific discovery, data analysis frequently follows a dual objective: the precise classification of well-characterized phenomena and the simultaneous identification of novel,

structurally distinct components. This challenge is ubiquitous in domains ranging from bioinformatics to astronomy, where vast datasets contain both known data instances and rare, unobserved events. While Supervised Learning excels at recovering known structures and Unsupervised Learning provides unbiased exploration, neither paradigm individually addresses this duality. Semi-Supervised Clustering (SSC) has emerged as the bridge between these extremes, aiming to improve partitioning accuracy by incorporating limited domain knowledge, typically in the form of pairwise constraints or labeled seeds (Basu and Mooney, 2005; Wagstaff et al., 2001).

However, a systematic review of the field reveals critical limitations in current SSC methodologies when applied to scientific novelty detection. The literature is predominantly driven by constraint-based methods utilizing must-link and cannot-link constraints (Basu et al., 2004b; Jiang et al., 2013). While effective for enhancing cluster purity, these methods typically operate under the assumption that the provided supervision is “representative” of the underlying data distribution (González-Almagro et al., 2023). This assumption forces algorithms to propagate constraints across the entire dataset, often distorting or suppressing the emergence of novel clusters that do not align with the priors. Furthermore, the majority of these frameworks, including variants of COP-KMeans and PC-KMeans, require the number of clusters (k) to be pre-specified (Wacquet et al., 2011; Xiong et al., 2014), a requirement that is fundamentally incompatible with the discovery of unanticipated structural components.

Alternative approaches, such as metric learning, attempt to reshape the feature space to satisfy constraints (Baghshah and Shouraki, 2010; Salunke et al., 2012). While powerful, these methods often struggle with local validity; a distance metric learned from a specific subset of known classes may not be applicable to the geometry of unknown regions. More recently, multi-stage frameworks have been proposed to address these rigidities. For instance, Śmieja et al. (2020) decompose clustering into binary classification and supervised grouping (S^3C^2), while Ienco and Pensa (2018) utilise multiresolution autoencoders to capture different granularities. Yet, even within these hybrid frameworks, the explicit decoupling of *known structure recovery* from *novelty discovery* remains under-explored.

The application domain further highlights this gap. While bioinformatics has seen extensive SSC application—particularly in gene expression and document clustering (Gu et al., 2013; Jiang et al., 2013), astronomical applications have received minimal explicit attention in the semi-supervised literature (Baumann and Hochbaum, 2022). This is a significant oversight, as current galactic surveys (e.g., *Gaia*, Gaia Collaboration et al. 2016) produce high-dimensional kinematic data in which known stellar streams coexist with undiscovered accretion remnants.

To address these limitations, we introduce CLiMB (CLustering in Multiphase Boundaries), a domain-informed novelty detection framework. CLiMB is motivated by the observation that separating constraint satisfaction from density-based exploration can resolve the tension between prior knowledge and novel discovery (Ienco and Interdonato, 2022). Unlike traditional methods that enforce global constraints, CLiMB operates via a sequential, two-phase architecture. The first phase, *K-Bound*, utilises customizable distance metrics (such as Euclidean, Mahalanobis, and custom metrics) and different boundaries to anchor clusters strictly to user-provided seed points. The second phase applies density-based clustering to

the unassigned residual data, enabling the detection of arbitrary, non-convex topologies without forcing them into the mold of the priors.

The application of the CLiMB framework to the *Gaia* Data Release 3 (DR3, Gaia Collaboration et al. 2023) catalog of RR Lyrae stars (RRLs) described in this paper yielded new insights into the dynamical architecture of the Milky Way (MW) halo. While traditional clustering approaches struggled with the sparsity of the dataset, CLiMB’s two-phase architecture proved robust when applied to the RRL sample. We demonstrate that CLiMB significantly outperforms heuristic and constraint-based baselines, such as C-DBSCAN (Ruiz et al., 2007) and heuristic SS-DBSCAN (Abdulhameed et al., 2024), in recovering known MW substructures while effectively identifying subtle dynamical features, such as Shakti and Shiva, which remain challenging for traditional methods. In the initial constrained phase, the algorithm not only recovered eight known substructures, such as the *Gaia* Sausage/Enceladus (GSE; Belokurov et al. 2018; Helmi et al. 2018) and Sequoia (Myeong et al., 2019; Matsuno et al., 2019), based on integral-of-motion similarity. The most significant outcome, however, emerged during the exploratory second phase: upon removing the known structures, the algorithm successfully unveiled three previously unassigned dynamical groups in the residual data. These corresponded to the Galactic Disk and the distinct accreted substructures Shiva and Shakti (Malhan and Rix, 2024). This ability to isolate novel features from the unlabelled field resulted in the characterization of 11 total substructures.

2 Methods

2.1 CLiMB: A Domain-Informed Novelty Detection Clustering Algorithm

In this work, we propose CLiMB (CLustering in Multiphase Boundaries), a novel clustering algorithm, called Domain-Informed Novelty Detection Clustering, designed to analyse datasets containing both known, well-characterized components and novelty regions where the discovery of new structures is crucial. Unlike traditional clustering methods that operate exclusively under unsupervised assumptions, our approach integrates prior domain knowledge (via “seed points”) with the capability to identify and group unexpected and innovative patterns.

The algorithm aims to overcome an inherent limitation in existing clustering approaches: the inability to effectively leverage partial domain knowledge while maintaining robustness in discovering previously unknown structures. Domain-Informed Novelty Detection Clustering is based on the premise that many real-world datasets contain both well-understood components, which can be guided by constraints, and unexplored regions that require adaptive discovery mechanisms. This is achieved through a sequential, two-phase architecture.

2.2 Phase 1: K-Bound, Constrained Clustering

The first phase, named *K-Bound*, implements a revised version of the K-means (McQueen, 1967) algorithm enhanced with multiple constraint mechanisms. Given a dataset $\mathbf{X} = \{\mathbf{x}_1, \mathbf{x}_2, \dots, \mathbf{x}_n\} \subset \mathbb{R}^d$ and a predefined number of constrained clusters k , *K-Bound* iteratively refines cluster centroids while enforcing three types of constraints.

- **Density Constraint:** To focus on well-defined regions, a point \mathbf{x}_i is only considered for assignment if its local density $\rho(\mathbf{x}_i)$ is above a specified threshold τ_ρ . The local density is calculated using a Gaussian kernel density estimate:

$$\rho(\mathbf{x}_i) = \frac{1}{n} \sum_{j=1}^n \exp \left(-\frac{d(\mathbf{x}_i, \mathbf{x}_j)^2}{2\sigma^2} \right)$$

where the density of a point \mathbf{x}_i is the sum of contributions from all other points in the dataset, and the contribution of each point \mathbf{x}_j decays smoothly in a Gaussian manner as its distance $d(\mathbf{x}_i, \mathbf{x}_j)$ increases. Kernel bandwidth, or σ , defines the scale of the neighborhood; a smaller σ considers only very close neighbors, while a larger σ results in a smoother density profile. A point \mathbf{x}_i is admitted for the constrained clustering phase only if its local density, $\rho(\mathbf{x}_i)$, satisfies the condition $\rho(\mathbf{x}_i) \geq \tau_\rho$. Points failing this condition are deferred to the exploratory phase.

- **Distance Constraint:** Following the density filter, a candidate point \mathbf{x}_i is evaluated for cluster assignment based on a strict proximity criterion. The assignment is contingent upon both identifying the nearest centroid and satisfying a maximum distance threshold, τ_d . We first determine the index of the nearest centroid, j^* , as:

$$j^* = \arg \min_{l \in \{1, \dots, k\}} d(\mathbf{x}_i, \mathbf{c}_l)$$

The formal assignment rule for the point's label, $L(\mathbf{x}_i)$, is then defined as:

$$L(\mathbf{x}_i) = \begin{cases} j^* & \text{if } d(\mathbf{x}_i, \mathbf{c}_{j^*}) \leq \tau_d \\ \text{unassigned} & \text{otherwise} \end{cases}$$

This constraint effectively imposes a boundary of constant metric radius τ_d around each centroid, defining the maximum spatial extent of a cluster. Its primary function is to enforce cluster compactness and prevent the inclusion of peripheral points that, while closer to one centroid than any other, may not be representative of the cluster's core structure. This ensures a high degree of intra-cluster affinity. Points that fail to satisfy this criterion, despite potentially residing in dense regions, are considered unassigned and are consequently passed to the exploratory phase for analysis.

- **Radial Constraint:** To prevent centroids from drifting excessively from their knowledge-guided initial positions, we enforce a radial constraint with threshold τ_r . The position of each centroid \mathbf{c}_j at iteration $t + 1$ is constrained relative to its initial position $\mathbf{c}_j^{(0)}$:

$$\|\mathbf{c}_j^{(t+1)} - \mathbf{c}_j^{(0)}\|_2 \leq \tau_r$$

This condition defines a permissible region of movement for each centroid. If an update calculation yields a position outside this region, the centroid is repositioned to the nearest point on the boundary, effectively capping its displacement. This radial constraint ensures robust convergence and guarantees that the final cluster definitions do not diverge substantially from the prior knowledge supplied to the algorithm.

2.2.1 ADVANCED INITIALIZATION AND METRIC FLEXIBILITY

K-Bound's effectiveness is enhanced by its sophisticated initialization and distance metric options.

Initialization Strategies: CLiMB supports multiple seed point mechanisms. Initialization can be random, or it can be guided by a list of initial centroid coordinates. For more granular control, the algorithm accepts a dictionary structure $\mathcal{S} = \{(\mathbf{c}_i, \mathbf{S}_i)\}_{i=1}^k$, where \mathbf{c}_i is the initial centroid coordinate and $\mathbf{S}_i = \{\mathbf{s}_{i,1}, \dots, \mathbf{s}_{i,m_i}\}$ is a set of associated seed points. The dictionary keys are used as the initial centroid positions, and after the algorithm converges, the points in \mathbf{S}_i are guaranteed to be assigned to cluster i , ensuring that prior knowledge is respected.

Metric Flexibility: CLiMB supports multiple distance metrics for the function $d(\cdot, \cdot)$:

- **Euclidean Distance:** $d(\mathbf{x}_i, \mathbf{x}_j) = \|\mathbf{x}_i - \mathbf{x}_j\|_2$.
- **Mahalanobis Distance:** $d(\mathbf{x}_i, \mathbf{x}_j) = \sqrt{(\mathbf{x}_i - \mathbf{x}_j)^T \mathbf{V}^{-1} (\mathbf{x}_i - \mathbf{x}_j)}$, where \mathbf{V} is the covariance matrix of the data.
- **Custom Metrics:** Users can define application-specific distance functions via a flexible interface.

2.3 Phase 2: Exploratory Novelty Detection

Points not assigned during the *K-Bound* phase form the set $\mathbf{X}_{\text{unassigned}}$. These points undergo exploratory clustering using density-based methods to discover novel, potentially non-convex patterns. CLiMB implements a strategy pattern, allowing for seamless integration of multiple algorithms, including DBSCAN (Ester et al., 1996), HDBSCAN (Campello et al., 2013, 2015), and OPTICS (Ankerst et al., 1999).

For the default DBSCAN-based exploration, two parameters are defined: a neighborhood radius ϵ and a minimum number of points MinPts. A point $\mathbf{x}_i \in \mathbf{X}_{\text{unassigned}}$ is identified as a core point if its ϵ -neighborhood contains at least MinPts points. Clusters are then formed by connecting core points and their neighbors. Labels assigned in this phase are indexed to be distinct from the constrained cluster labels.

2.4 Convergence, Complexity, and Implementation

2.4.1 CONVERGENCE CRITERIA

The iterative nature of the K-Bound phase requires a robust set of criteria to determine when a stable and meaningful cluster configuration has been achieved. The process is designed to terminate when the cluster assignments and centroid positions no longer exhibit significant changes. This is governed by two distinct conditions.

The first condition for termination is based on the principle of centroid stability. The iterative refinement process is considered to have converged when the displacement of all centroids between two consecutive iterations becomes negligible. We quantify this by monitoring the maximum displacement observed across all centroids. Specifically, the algorithm halts when the largest distance between a centroid's position at iteration t , $\mathbf{c}_j^{(t)}$, and its

updated position at iteration $t + 1$, $\mathbf{c}_j^{(t+1)}$, falls below a user-defined tolerance threshold, τ_c . This condition is expressed formally as:

$$\max_{j \in \{1, \dots, k\}} \|\mathbf{c}_j^{(t+1)} - \mathbf{c}_j^{(t)}\|_2 < \tau_c$$

This use of the maximum displacement provides a conservative criterion. It ensures that the entire system has stabilized, as even the most mobile centroid has settled. The tolerance parameter τ_c is a hyperparameter that balances the trade-off between the precision of the final centroid placement and the total computational cost; a smaller τ_c leads to a more refined solution at the expense of a potentially higher number of iterations.

To guarantee termination under all circumstances, a secondary criterion is implemented. The algorithm will halt if it reaches a predefined maximum number of iterations, max_iter . This condition is crucial to prevent cases of non-convergence, such as oscillations where centroids shift between a finite set of positions in successive iterations without ever meeting the stability criterion. This ensures that the algorithm always terminates in a finite amount of time, providing a deterministic upper bound on its runtime.

2.4.2 COMPUTATIONAL COMPLEXITY

The computational complexity of the CLiMB algorithm is analyzed by considering its two sequential phases. The runtime of the *K-Bound Phase* is characterized as $O(t \cdot n \cdot k \cdot d)$, where t is the number of iterations, n is the number of data points, k is the number of clusters, and d is the feature space dimensionality. This complexity arises from the iterative core of the algorithm. Within each iteration, the primary computational complexity is the *Label Assignment* phase. This step requires computing the distance between each of the n points and all k centroids, resulting in an $n \times k$ distance matrix. This operation has a cost of $O(n \cdot k \cdot d)$. The subsequent *Centroid Update* phase, where new cluster means are calculated, is less costly, with a complexity of $O(n \cdot d)$. As the assignment phase is dominant, it dictates the complexity of a single iteration. Additionally, it is important to note a one-time pre-computation cost of $O(n^2 \cdot d)$ for the initial density estimation, which can be a significant factor for datasets with a large number of samples. Comparing the two phases within an iteration, the Label Assignment ($O(n \cdot k \cdot d)$) is computationally more expensive than the Centroid Update ($O(n \cdot d)$). Therefore, the complexity of a single iteration is governed by the Label Assignment phase.

The complexity of the subsequent *Exploratory Phase* is contingent upon the chosen algorithm and the number of unassigned points, $n' \leq n$. The default algorithm, DBSCAN, typically exhibits an average-case complexity of $O(n' \log n')$ when optimized with spatial indexing structures. For the alternative supported algorithms, such as OPTICS and HDBSCAN, the worst-case computational complexity is $O((n')^2)$. While computationally more intensive, these methods provide more sophisticated models for density-based discovery, which can be advantageous for complex data structures.

In most practical applications, the runtime of the K-Bound phase constitutes the dominant portion of the total computational cost, particularly when the number of constrained clusters k is non-trivial and the number of unassigned points n' is significantly smaller than the total sample size n .

2.4.3 IMPLEMENTATION DETAILS

CLiMB is implemented in Python and is compatible with the *scikit-learn*¹ ecosystem. The modular architecture allows for easy extension. For flexible parameter configuration, the algorithm employs a builder design pattern. This design facilitates systematic parameter tuning and enhances experimental reproducibility. The package also includes comprehensive 2D and 3D visualization tools. The source code is publicly available under the MIT license and is hosted on GitHub², where documentation, tests and examples are also provided. The algorithm’s implementation prioritizes computational efficiency by exploiting optimized, vectorized operations provided by the NumPy³ and SciPy⁴ libraries for all distance calculations and array manipulations. Memory usage is managed by recalculating intermediate data structures, such as the distance matrix, within each iteration, thus avoiding the storage of a complete computational history. The pseudo-code is presented in Algorithm 1.

Algorithm 1 The CLiMB Algorithm

1: **Input:** Dataset \mathbf{X} , number of clusters k , thresholds $\tau_\rho, \tau_d, \tau_r, \tau_c$
 Seed points \mathcal{S} (optional), Exploratory algorithm A_{expl}

Phase 1: Constrained Clustering (K-Bound)

2: Initialize centroids $\mathbf{C}^{(0)} = \{\mathbf{c}_1^{(0)}, \dots, \mathbf{c}_k^{(0)}\}$ using \mathcal{S} or randomly.
 3: Compute local density $\rho(\mathbf{x}_i)$ for all $\mathbf{x}_i \in \mathbf{X}$.
 4: **for** $t = 0, \dots, \text{max_iter}$ **do**
 5: Assign labels: $L_i \leftarrow \arg \min_j d(\mathbf{x}_i, \mathbf{c}_j^{(t)})$ if $\rho(\mathbf{x}_i) \geq \tau_\rho$ and $d(\mathbf{x}_i, \mathbf{c}_j^{(t)}) \leq \tau_d$.
 6: Update centroids $\mathbf{C}^{(t+1)}$ based on the mean of assigned points.
 7: Enforce radial constraint: $\|\mathbf{c}_j^{(t+1)} - \mathbf{c}_j^{(0)}\|_2 \leq \tau_r$.
 8: **if** $\max_j \|\mathbf{c}_j^{(t+1)} - \mathbf{c}_j^{(t)}\|_2 < \tau_c$ **then break**
 9: **end if**
 10: **end for**
 11: Let $\mathbf{X}_{\text{unassigned}}$ be the set of unassigned points.

Phase 2: Exploratory Clustering

12: **if** $\mathbf{X}_{\text{unassigned}}$ is not empty **then**
 13: Run A_{expl} on $\mathbf{X}_{\text{unassigned}}$ to get exploratory labels L_{expl} .
 14: Combine constrained and exploratory labels.
 15: **end if**
 16: **Output:** Final cluster labels for all points in \mathbf{X} .

3 Related Works

Semi-supervised clustering (SSC) constitutes a critical subfield of machine learning that addresses the inherent ill-posedness of unsupervised clustering by incorporating limited

1. <https://scikit-learn.org>
 2. <https://github.com/LorenzoMonti/CLiMB>
 3. <https://numpy.org/>
 4. <https://scipy.org/>

supervisory information into the partitioning process. This supervision, typically manifested as class labels for a data subset or as pairwise constraints (i.e., must-link and cannot-link pairs), serves to regularize the problem, guiding the algorithm toward a semantically meaningful solution that aligns with available domain knowledge as described in Qin et al. (2019). The evolution of SSC methodologies reveals a trajectory from direct algorithmic modifications to more sophisticated data-space transformations and, ultimately, to hybrid multi-stage frameworks. This review charts this evolution to identify persistent challenges and contextualize the contribution of our proposed algorithm, CLiMB.

3.1 Evolution of Methodological Paradigms in SSC

The primary paradigms for integrating supervision in clustering can be broadly categorized into two major approaches: direct modification of the clustering algorithm and transformation of the underlying data representation. Early work predominantly focused on the former. One foundational strategy involves informed initialization, or seeding, where labeled data points are used to define the initial cluster centroids. By commencing the iterative optimization process from a more favorable position in the solution space, such methods mitigate the risk of convergence to suboptimal local minima, thereby enhancing both the accuracy and stability of the final partition (Basu et al., 2002).

A more flexible form of algorithmic-level integration is realized through constraint-based clustering. Foundational algorithms like Cop-Kmeans (Wagstaff et al., 2001) modify the cluster assignment step to enforce must-link and cannot-link constraints procedurally. This principle was later formalized more rigorously through the modification of the clustering objective function, as exemplified by PCKmeans (Basu et al., 2004a), and has been successfully extended to other clustering families, including hierarchical and spectral methods (Davidson and Ravi, 2005). This line of work continues to evolve, as seen in Yang et al. (2012), who introduce ICop-Kmeans, an enhanced variant that addresses constraint violations by leveraging object certainty and weighted co-association, further integrated with a novel constrained self-organizing map to refine semi-supervised clustering. This paradigm was also adapted for density-based algorithms, which are inherently better suited for discovering non-globular clusters. For instance, C-DBSCAN first partitions the data into numerous local micro-clusters while strictly respecting cannot-link constraints, and only subsequently merges these based on must-link constraints and proximity (Ruiz et al., 2007).

A distinct but related approach involves modifying algorithmic behavior not with specific pairwise constraints, but with domain-guided heuristics. Instead of providing examples, this paradigm injects general rules based on domain knowledge to guide the clustering process. The heuristic SS-DBSCAN method, inspired by the work of Abdulhameed et al. (2024), exemplifies this by altering the core point selection criteria of DBSCAN. In this model, a point can only initiate a new cluster if it is both in a dense region and satisfies an external, user-defined "importance" function. While this allows for the integration of high-level domain knowledge, the effectiveness of such methods is highly dependent on the quality and generalizability of the handcrafted heuristic rule.

A subsequent and significant shift in SSC research moved beyond algorithmic adaptation to focus on clustering metric learning. Instead of modifying the clustering process, this paradigm aims to learn a distance metric under which the data's geometric structure

inherently conforms to the supervisory information. The seminal work by Xing et al. (2002) framed this as a convex optimization problem to learn a Mahalanobis distance metric that minimizes distances between must-link pairs while maximizing them for cannot-link pairs. The power of this approach lies in its ability to reshape the feature space topology as in Ye et al. (2007); Zhang et al. (2012), often leading to superior performance as the subsequent application of even a simple clustering algorithm can yield accurate results. This concept remains highly relevant, with modern deep clustering methods like Semi-Supervised Deep Embedded Clustering (SDEC) employing pairwise constraints to regularize the learned latent embedding space, thereby ensuring that the learned features are discriminative and well-suited for clustering (Ren et al., 2019).

The limitations of these single-phase approaches, particularly their sensitivity to noisy supervision and their rigidity in discovering previously unseen cluster structures, motivated the development of multi-step and hybrid frameworks. These more advanced methods often decouple the clustering process into distinct stages of supervision-guided partitioning and unconstrained exploration. For example, active learning frameworks refine an initial clustering by interactively querying for constraints on the most ambiguous data points (Grira et al., 2008). Other adaptive methods employ a multi-stage process wherein parameters for a density-based clustering algorithm are determined using both labeled and unlabeled data prior to the final partitioning (Yang et al., 2017). As a comprehensive survey by Cai et al. (2023) highlights, the field is replete with diverse techniques, but this trend toward multi-stage processing indicates a growing recognition of the need for more flexible and robust algorithmic designs.

3.2 Persistent Challenges and Identified Research Gaps

Despite considerable progress, the efficacy of existing SSC algorithms is predicated on several key assumptions, the violation of which exposes persistent challenges. A primary issue is the reliability of the supervisory signal. The majority of algorithms presuppose that provided labels and constraints are accurate, an assumption that is frequently untenable in real-world applications. While “safe” SSC methods have been proposed to mitigate the impact of noisy supervision, for instance by assigning confidence weights to labeled instances (Gan et al., 2019), this remains an open and critical research area.

Furthermore, a fundamental tension exists in the trade-off between exploitation and exploration, that is, between adhering to the provided supervision and discovering the intrinsic structure of the unlabeled data. Over-reliance on strong constraints can lead to a model that satisfies the supervision but fails to capture novel or emergent clusters, effectively constraining the discovery process. This exposes a critical gap in the literature: the absence of a unified framework designed explicitly to operate on datasets containing both well-characterized and entirely novel components. Current methods implicitly assume that the limited supervision is representative of the global class distribution. They lack a formal mechanism to first isolate and model the “known” data components based on supervision, and then perform unconstrained, exploratory clustering on the residual data. This limitation is particularly acute in domains such as network security, where known attack signatures must be identified alongside novel threats, or in bioinformatics, where new cell types are discovered from datasets containing previously annotated ones.

Our work, CLiMB, is designed to directly address this gap. It introduces a sequential, two-phase architecture that systematically decouples the exploitation of prior knowledge from the exploratory discovery of unknown patterns. By first partitioning the data space according to supervisory seeds and subsequently applying an unconstrained clustering algorithm to the remaining data, CLiMB provides a principled solution for clustering in multi-phase boundaries where both confirmation and discovery are required.

4 Experiments

To validate the performance and robustness of our proposed framework, we designed a comprehensive experimental evaluation. Our primary goal is to demonstrate that CLiMB’s two-phase, adaptive-metric architecture offers a superior solution for *domain-informed novelty detection clustering* compared to existing semi-supervised methods. The experiments are structured to assess not only the overall clustering quality but also to independently evaluate the distinct contributions of CLiMB’s constrained knowledge-recovery phase and its unsupervised exploratory discovery phase

The primary case study is drawn from the domain of Galactic archaeology, a field where identifying sparsely distributed stellar structures within massive, noisy datasets presents a significant challenge perfectly aligned with the problem CLiMB is designed to solve. We benchmark CLiMB against alternative density-based semi-supervised algorithms, evaluating their performance on a real-world dataset of RRLs from the *Gaia* DR3. The following sections detail the dataset, the comparative methodology, and the evaluation results.

4.1 Galactic Archaeology with RRLs from Gaia DR3

RRLs are pulsating variable stars, serving as ideal tracers of old, metal-poor stellar populations prevalent in the MW halo. RRLs are excellent standard candles for measuring distances due to their well-defined luminosity-metallicity relations in the visual bands and period-luminosity-metallicity relations in the near- and mid-infrared bands (e.g., Longmore et al. 1986; Clementini et al. 2003; Bono et al. 2003; Sollima et al. 2008; Muraveva et al. 2018). Additionally, RRLs are effective metallicity tracers, as their metallicity can be estimated from photometric parameters, such as the pulsation period and Fourier decomposition parameters of their light curves, without requiring spectroscopic data (e.g., Jurcsik and Kovacs 1996; Morgan et al. 2007; Muraveva et al. 2025). As remnants tracers of ancient stellar systems, RRLs are particularly valuable for studying the dynamical history of the Galaxy, including past accretion events that have shaped its halo (Massari et al., 2019; Helmi, 2020). These events, involving the merger of dwarf galaxies or globular clusters, leave kinematic and spatial signatures in the form of stellar streams and substructures, which can be traced using integrals of motion, such as the total energy (E), the angular momentum along the Z -axis (L_z), and the perpendicular component of angular momentum (L_\perp) (Helmi and Tim de Zeeuw, 2000; Ceccarelli et al., 2024; Dodd et al., 2023).

The *Gaia* mission (Gaia Collaboration et al., 2016), launched by the European Space Agency in 2013, has revolutionized Galactic astronomy by providing unprecedented astrometric, photometric, and spectroscopic data for over a billion stars. In both Muraveva et al. (in prep.) and the present study, we selected a sample of 4,933 RRLs, as shown in Figure 1, for which positions, proper motions, parallaxes, and radial velocities are available in *Gaia*

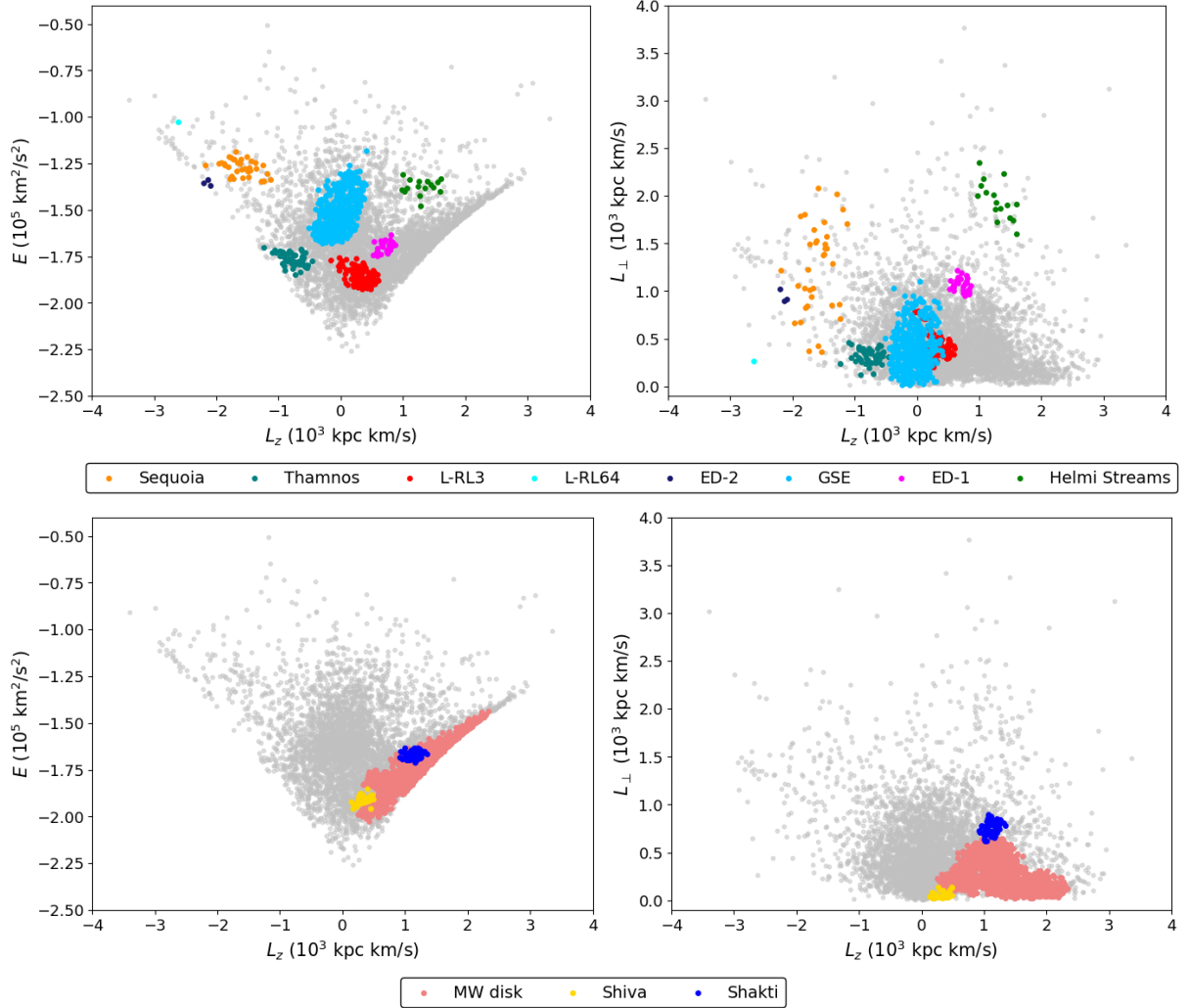


Figure 1: Distribution of 4,933 RRLs from *Gaia* DR3 in the E - L_z and L_z - L_{\perp} planes, colour-coded by the substructure to which they belong. Grey dots indicate RRLs not assigned to any substructure. The top panels show RRLs identified by the CLiMB algorithm in known MW substructures from Dodd et al. (2023), while the bottom panels show substructures not reported by Dodd et al. (2023), discovered during the exploratory phase of the CLiMB algorithm.

DR3. We then used this six-dimensional phase-space information to compute integrals of motion and applied clustering algorithms to identify dynamical substructures in the MW halo associated with past accretion events.

From a machine learning perspective, we project this high-dimensional physical data into a compact 3-dimensional feature space $\mathbf{X} \in \mathbb{R}^{n \times 3}$. This space defines the dynamical manifold of the stellar streams and constitutes the actual input for our clustering framework:

1. **Angular Momentum (L_z)**: The component of angular momentum along the Galactic Z -axis.
2. **Total Energy (E)**: The orbital energy of the star.
3. **Perpendicular Angular Momentum (L_\perp)**: The component of angular momentum perpendicular to the rotation axis ($L_\perp = \sqrt{L_x^2 + L_y^2}$), which effectively traces the inclination of the orbit.

This feature space is notoriously difficult for clustering due to the varying densities of the streams and the non-Gaussian nature of the background noise.

4.2 Data Preparation and Preprocessing

To prepare the raw astrophysical data for the semi-supervised pipeline, we implemented a specific preprocessing routine to mitigate biases and ensure isotropic metric properties.

Energy Decorrelation: Systematic biases in energy estimation can introduce artificial correlations. To mitigate this, we applied a statistical shuffling technique. We generated 1,000 permutations of the energy feature vector \mathbf{e} ; the mean of these shuffled vectors was then subtracted from the original energy values:

$$\mathbf{e}' = \mathbf{e} - \mathbb{E}[\text{shuffle}(\mathbf{e})]_{1000}$$

This procedure effectively removes the mean background energy level while preserving local kinematic structures.

Scaling: Given the heterogeneous ranges of the features (L_z and L_\perp in kpc km/s, E in km^2/s^2), the dataset was standardized using Z-score normalization (zero mean, unit variance) via `StandardScaler` to ensure isotropic distance calculations in the clustering phase.

Supervisory Signal Generation: Ground truth labels for a subset of the data were derived from the catalogue of Dodd et al. (2023), identifying 8 known substructures (e.g., GSE, Sequoia). To simulate a realistic semi-supervised scenario and generate robust inputs for the algorithms (Seeds for CLiMB, Must-Link/Cannot-Link for baselines), we employed a radial sampling strategy:

1. For each known cluster, we calculated the centroid in the scaled feature space.
2. Member points were sorted by their Euclidean distance to the centroid.

3. We sampled a percentage of points (defaulting to 90% for the main benchmark, and varying from 10% to 100% for sensitivity analysis) using stratified sampling along this radial distribution.

This strategy ensures that the supervisory signals are representative of the cluster’s spatial extent, providing a fair test of the algorithms’ ability to generalize from core samples to peripheral members.

4.3 Comparative Benchmark with Alternative Semi-Supervised Methods

The selection of benchmark algorithms was guided by the intrinsic characteristics of the domain of astrophysical problems. Stellar structures in the Galactic halo, such as streams and associations, especially, traced by the relatively sparse RRLs, are often filamentary, and exhibit widely varying densities, embedded within a large, unstructured background of field stars. These properties render traditional partitional clustering algorithms, like K-Means, fundamentally unsuitable. Such methods typically require the number of clusters, k , to be specified a priori, contrary to our goal of discovering novel structures, and tend to discover only convex or globular-shaped clusters, failing to capture the irregular morphologies of galactic substructures.

For these reasons, our benchmark focuses exclusively on the family of density-based clustering algorithms. These methods are uniquely suited to this problem as they can identify clusters of arbitrary shape, don’t require a predefined number of clusters, and can naturally distinguish meaningful structures from low-density noise. To provide the most relevant and challenging comparison for CLiMB, we selected two alternative semi-supervised algorithms from this family, specifically chosen because they represent distinct and fundamentally different philosophies for integrating prior knowledge:

- **Heuristic SS-DBSCAN:** This approach, is based on the publicly available code from Zaki⁵, which corresponds to the method described in Abdulhameed et al. (2024), that modifies the cluster expansion mechanism of DBSCAN. Although the standard DBSCAN expands through any core point, this variant allows a core point to propagate the cluster label only if it satisfies a domain-specific “importance” function $\mathcal{I}(\mathbf{x})$. Based on the physical properties of accreted halo stars, we implemented $\mathcal{I}(\mathbf{x})$ to select stars that reside in the kinematic tails of the distribution. Specifically, a point is considered important if its angular momentum L_z is in the bottom 15% of the range (retrograde/low-rotation) or its total energy E is in the top 15% (high-energy). This represents a *top-down, static supervision* paradigm designed to filter out background field stars.
- **C-DBSCAN (Constraint-based DBSCAN):** This algorithm exemplifies the classic *bottom-up, constraint-based* supervision paradigm. It operates in multiple stages by first creating cautious, local micro-clusters that respect Cannot-Link constraints, and subsequently merging them based on Must-Link constraints and proximity. Our implementation was developed to follow the original algorithm described by Ruiz et al. (2007).

5. https://github.com/TibaZaki/SS_DBSCAN

By benchmarking against these two methods, we test CLiMB’s performance against both a top-down, domain-guided approach and a bottom-up, constraint-based approach. The prior knowledge of the 8 known substructures was used to generate seed points for CLiMB, define the heuristic rule for SS-DBSCAN (based on extreme kinematic properties), and generate Must-Link/Cannot-Link constraints for C-DBSCAN. To ensure a fair comparison, a hyperparameter optimization was performed for each algorithm to find its optimal configuration before the final benchmark execution. (see Appendix A for details).

4.4 Evaluation Methodology

To provide a comprehensive and fair assessment, we designed an evaluation strategy that addresses the specific challenges of our astrophysical dataset. Given that our ground truth is incomplete, containing a large set of 4,465 unclassified “field stars”, a single global metric is insufficient and potentially misleading. Our evaluation is therefore structured into three distinct analyses.

First, we conduct a detailed analysis of knowledge recovery. The primary goal is to measure how effectively each semi-supervised algorithm reconstructs the known substructures when provided with prior knowledge. For this, we evaluate performance exclusively on the subset of data corresponding to the 8 known clusters. We use the Adjusted Rand Index (ARI) defined by Hubert and Arabie (1985), as the main performance score, supplemented by homogeneity and completeness as diagnostic metrics (Rosenberg and Hirschberg (2007)). These allow us to distinguish between algorithms that erroneously merge distinct substructures (low homogeneity) and those that unnecessarily fragment them (low completeness). For CLiMB, this evaluation is performed on the output of its first (constrained) phase to specifically isolate the performance of its knowledge-anchoring mechanism.

Second, we assess the quality of exploratory discovery. This analysis focuses on the new clusters identified by each algorithm from the unclassified field stars. Since no ground truth exists for these potential discoveries, we employ a qualitative and domain-based validation. We utilize phase-space diagnostic plots to verify that the newly identified clusters form coherent, dense morphologies (E, L_z, L_{\perp}) distinct from the background noise. Furthermore, we cross-reference these discoveries with recent astrophysical literature (Malhan and Rix, 2024) to confirm their physical plausibility.

Finally, we perform a sensitivity analysis to understand how robust each algorithm is to the amount of supervision. We systematically vary the percentage of known points used as seeds (from 10% to 100%) and measure the resulting ARI on the known-data subset. This experiment reveals how efficiently each algorithm leverages prior knowledge, distinguishing between methods that learn monotonically and those that stagnate.

5 Results and Discussion

Our experimental evaluation demonstrates that CLiMB consistently and significantly outperforms the alternative semi-supervised methods across all aspects of the analysis. The results not only establish the superiority of our proposed framework but also provide key insights into the strengths of its two-phase, adaptive-metric architecture.



Figure 2: Visual benchmark of clustering results on the known subset of structures. In all panels, distinct colors represent separate cluster assignments. Top-Left: Partial ground truth for the 8 significant substructures. Top-Right: CLiMB output (ARI: 0.829) showing accurate recovery of complex, non-convex shapes. Bottom-Left: Heuristic SS-DBSCAN (ARI: 0.040) fails to form coherent structures, fragmenting streams into noise. Bottom-Right: C-DBSCAN (ARI: 0.152) suffers from massive over-merging, collapsing distinct kinematic streams into a single macro-cluster.

5.1 Knowledge Recovery and Baseline Comparison

We first assess the ability to reconstruct the 8 known substructures using the full set of available constraints. Figure 2 presents a visual comparison between the ground truth and the final clustering outputs.

As shown in Table 1, CLiMB achieves an Adjusted Rand Index (ARI) of 0.829 (at 90% supervision), producing a partition that closely mirrors the topological complexity of the ground truth. The high *Homogeneity* score (0.953) confirms that the Mahalanobis-based anchoring effectively prevents the "leaking" of centroids into neighboring distinct structures.

In stark contrast, the baselines exhibit critical failure modes. C-DBSCAN (Figure 2, Bottom-Right) achieves an ARI of only 0.152. The visualization reveals that its bottom-up constraint propagation is prone to "chain-reaction" merging in high-density regions, obliterating the boundaries between distinct stellar streams. Similarly, Heuristic SS-DBSCAN (Figure 2, Bottom-Left) yields an ARI of 0.040, demonstrating that a single global density-heuristic is insufficient to capture the varying morphologies of galactic substructures.

Table 1: Performance on Knowledge Recovery (8 known substructures). CLiMB is compared against the final output of baselines. Bold denotes best performance.

Algorithm	ARI	Homogeneity	Completeness
CLiMB	0.829	0.953	0.783
Heuristic SS-DBSCAN	0.040	0.024	0.465
C-DBSCAN	0.152	0.169	0.250

5.2 Exploratory Discovery Performance

The second evaluation assessed the quality of new clusters discovered within the 4,465 out of 4,933 unclassified field stars. This test measures the algorithm's ability to perform meaningful novelty detection beyond the initial constraints. CLiMB demonstrates a robust capability in isolating latent structures. Its exploratory phase successfully identified three distinct, geometrically coherent groups in the residual data. As visually confirmed by the diagnostic plot in Figure 3, these new clusters (represented by warm-colored crosses) are not mere stochastic noise; they occupy well-defined, high-density regions of the (E - L_z) phase space and are clearly separable from the constrained clusters (cool-colored circles). Subsequent domain analysis confirms that these groups correspond to the Galactic Disk and the recently hypothesized *Shiva* and *Shakti* substructures (Malhan and Rix, 2024), validating the physical significance of the resulting partition. In contrast, the baselines failed to produce comparable insights. As seen in the comparison panel (Figure 2), C-DBSCAN failed to identify these novelties, merging the majority of the field stars into the known structures or classifying them as noise. Heuristic SS-DBSCAN produced fragmented, incoherent groupings that do not align with known kinematic morphologies. This confirms that without the "cleaning" effect of CLiMB's first phase, standard density-based methods struggle to distinguish subtle novel signals from the dominant background noise.

5.3 Overall Performance and Sensitivity to Supervision

The final analysis considers the overall performance and robustness. The "Global Meaningful ARI" confirms CLiMB's lead with a score of 0.829, compared to 0.040 for SS-DBSCAN and 0.152 for C-DBSCAN.

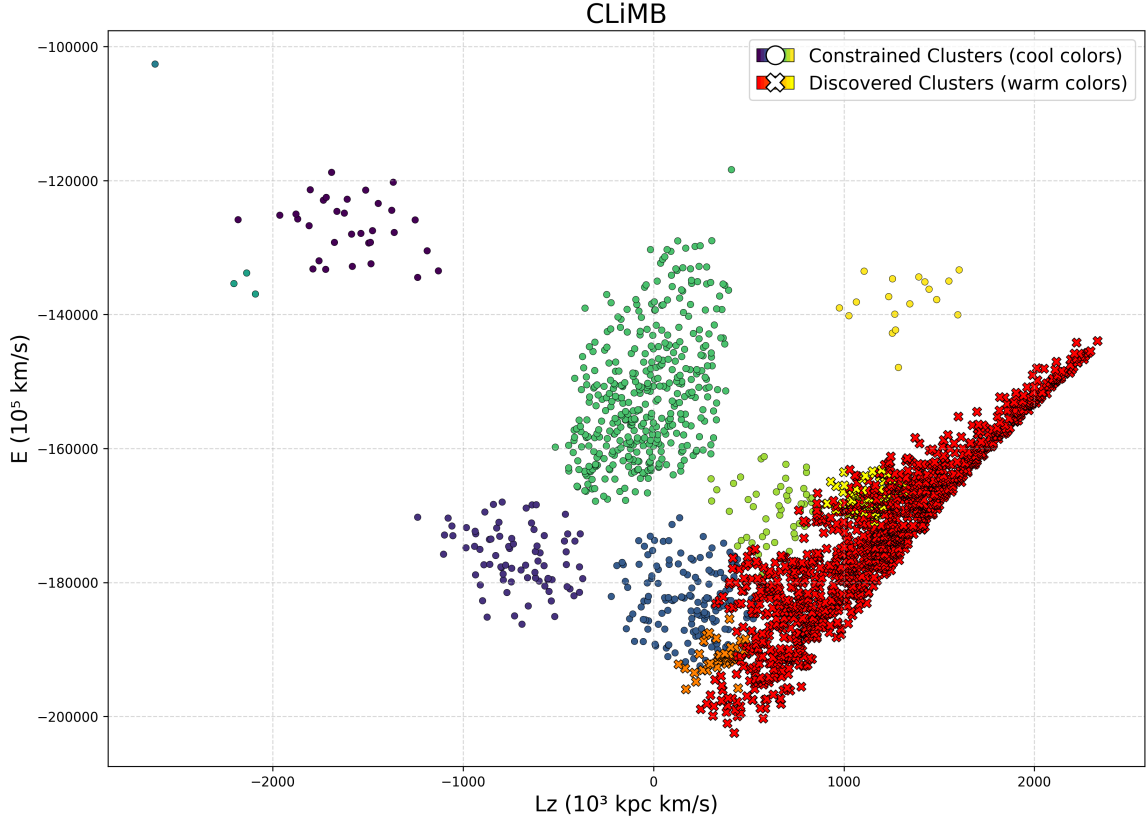


Figure 3: Diagnostic plot of CLiMB’s final result in the E - L_z plane. Points are categorized by both shape and color to distinguish the algorithmic phases: circles in cool colors represent structures recovered during the constrained phase (Phase 1), while crosses in warm colors denote clusters identified during the exploratory phase (Phase 2). This diagnostic validates the detection of the *Shiva* (orange) and *Shakti* (yellow) structures, as well as the Galactic Disk (red), all recovered as exploratory discoveries.

Furthermore, the sensitivity analysis, shown in Figure 4, highlights CLiMB’s remarkable robustness and efficiency in learning from prior knowledge. A crucial divergence in algorithmic behavior is observed: while C-DBSCAN and SS-DBSCAN exhibit stagnant performance regardless of the amount of supervision (flat lines), CLiMB demonstrates a strict monotonic improvement. Notably, even with sparse prior knowledge (10% of seeds), CLiMB achieves an ARI (≈ 0.32) that doubles the performance of the best baseline, scaling up to 0.829 as more information is provided.

This demonstrates that CLiMB’s architecture effectively translates extensive domain knowledge into topological accuracy without becoming over-constrained, a key advantage over traditional methods that fail to leverage additional labels.

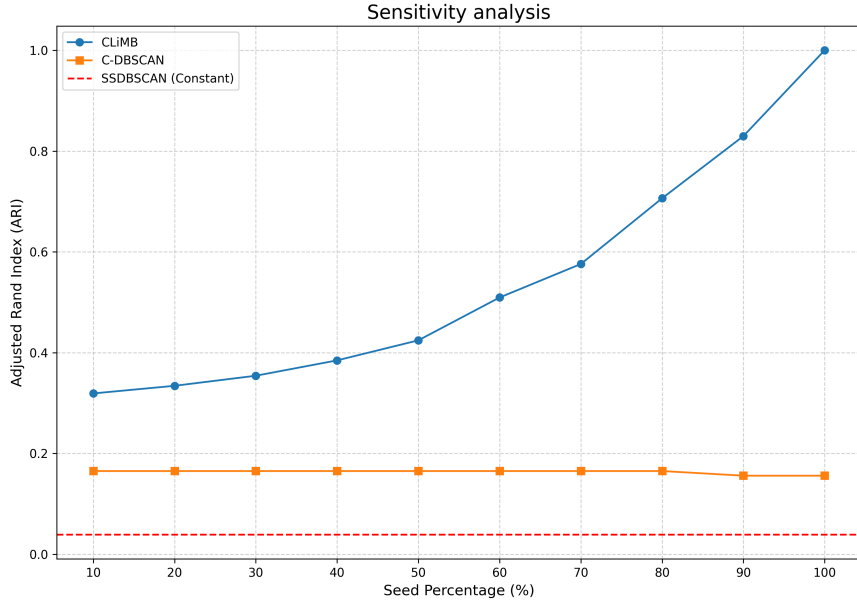


Figure 4: Sensitivity analysis showing the Adjusted Rand Index (ARI) on knowledge recovery as a function of the percentage of prior knowledge (10% to 100%). CLiMB (blue) demonstrates monotonic learning and high performance even with limited supervision, whereas baselines (C-DBSCAN and SSDBSCAN in orange and red) stagnate.

5.4 Limitations and Operational Trade-offs

While CLiMB demonstrates superior accuracy and discovery capabilities, these advantages come with specific operational trade-offs regarding configuration and complexity.

First, the dual-phase architecture inherently expands the hyperparameter space compared to monolithic algorithms. Beyond the standard density parameters (ϵ , MinPts) required for the exploratory phase, the constrained phase necessitates the definition of specific anchoring thresholds, namely density (τ_ρ), distance (τ_d), and radial drift (τ_r). While this offers granular control, it requires a hierarchical optimization strategy as detailed in Appendix A. Second, as analyzed in Section 2.4.2, the reliance on Gaussian Kernel Density Estimation for the initial filtering introduces a pre-computation cost of $O(n^2d)$ in the naive implementation. While the iterative assignment phase is efficient, this initialization step represents the computational bottleneck for large datasets, necessitating the use of approximation structures (e.g., kd-trees) for samples exceeding millions of points. Finally, the architectural decoupling introduces a sequential dependency: the quality of the Novelty Detection is strictly conditional on the successful anchoring of the first phase. If the constrained constraints are too lax, novelties may be absorbed into known clusters; if too strict, known points may leak into the residual space, contaminating the discovery process.

6 Conclusions

In this work, we introduced CLiMB, a domain-informed novelty detection framework designed to resolve the fundamental challenge in semi-supervised clustering: balancing the adherence to prior knowledge with the flexibility to discover unanticipated structures. By architecturally decoupling the problem into a constrained anchoring phase (*K-Bound*) and a density-based exploratory phase, CLiMB overcomes the “representativeness” assumption that limits traditional constraint-based methods. This separation allows practitioners to rigidly enforce known physical or biological constraints where data is well-characterized, while retaining the mathematical freedom to detect non-convex, topological anomalies in the unlabelled residual data.

The practical efficacy of this approach was demonstrated through a challenging application in Galactic archaeology using *Gaia* DR3 data. CLiMB achieved a significant performance advantage over existing semi-supervised baselines, demonstrating robust learnability by scaling to an ARI of 0.829, whereas competitor methods stagnated below 0.20 regardless of the supervision level. Beyond metric performance, the framework facilitated genuine scientific discovery: the algorithm’s ability to ”clean” the feature space in the first phase allowed for the isolation of the *Shiva* and *Shakti* substructures, along with the Galactic Disk, from the residual background. These results underscore CLiMB’s potential as a hypothesis generation tool for high-dimensional scientific domains where valid signals are sparse and the catalogue of known phenomena is incomplete.

Despite these advancements, the current framework exhibits specific limitations that outline the path for future research. First, the dual-phase architecture introduces a higher dimensionality in the hyperparameter space compared to monolithic algorithms; while partially mitigated by our hierarchical optimization strategy, the dependence on user-defined thresholds (τ_p, τ_d, τ_r) assumes some domain intuition regarding cluster scales. Second, the computational complexity of the initial Gaussian density estimation ($O(n^2d)$) poses scalability challenges for datasets exceeding millions of points, necessitating the future integration of approximate nearest-neighbor methods (e.g., kd-trees). Finally, the sequential nature of the algorithm implies that the exploratory phase is sensitive to the quality of the initial constrained assignment; future iterations could explore a joint optimization objective that refines both phases simultaneously to minimize leakage.

Acknowledgments and Disclosure of Funding

Support to this study has been provided by INAF Mini-Grant (PI: Tatiana Muraveva), by the Agenzia Spaziale Italiana (ASI) through contract ASI 2018-24-HH.0, its Addendum 2018-24-HH.1-2022 and contract ASI 2025-10-H.00, and by Premiale 2015, MIning The Cosmos - Big Data and Innovative Italian Technology for Frontiers Astrophysics and Cosmology (MITiC; P.I.B.Garilli). This work uses data from the European Space Agency mission *Gaia* (<https://www.cosmos.esa.int/gaia>), processed by the *Gaia* Data Processing and Analysis Consortium (DPAC; <https://www.cosmos.esa.int/web/gaia/dpac/consortium>). Funding for the DPAC has been provided by national institutions, in particular the institutions participating in the *Gaia* Multilateral Agreement. More information about this disclosure can be found on the JMLR website.

Appendix A. Hyperparameter Optimization

To ensure a fair and robust comparison, a hyperparameter optimization process was conducted for each algorithm prior to the final benchmark execution. The primary objective of this process was to identify the optimal parameter configuration for each method on our specific dataset. For the density-based competitors (Heuristic SS-DBSCAN and C-DBSCAN), we performed a grid search over a range of values for `eps` and `min_samples`, selecting the combination that maximized the "Global ARI" as described in the main text.

For our proposed algorithm, CLiMB, we employed a hierarchical, two-stage optimization strategy tailored to its architecture:

1. **Phase 1 (Constrained) Optimization:** We first optimized the parameters governing the knowledge-recovery phase (`density_threshold`, `distance_threshold`, etc.) by maximizing the ARI calculated exclusively on the subset of 8 known substructures.
2. **Phase 2 (Exploratory) Optimization:** Using the optimal parameters from the first stage, we then optimized the exploratory parameters (`eps`, `min_samples`) by minimizing the Davies-Bouldin Index (DBI) (Davies and Bouldin, 2009) on the clusters discovered within the unclassified data.

This hierarchical approach ensures that each phase of CLiMB is fine-tuned for its specific task. The final, optimal hyperparameters used for the benchmark analysis presented in this paper are detailed in Table 2. The complete code for the optimization routines, along with the scripts to reproduce all results, is publicly available in our GitHub repository⁶.

Table 2: Optimal Hyperparameters Used in the Benchmark.

Algorithm	Parameter	Optimal Value
CLiMB	<i>Phase 1 (Constrained)</i>	
	<code>density_threshold</code>	0.005
	<code>distance_threshold</code>	0.5
	<code>radial_threshold</code>	0.1
	<code>convergence_tolerance</code>	0.01
	<i>Phase 2 (Exploratory)</i>	
	<code>eps</code>	0.190
	<code>min_samples</code>	24
Heuristic SS-DBSCAN	<code>eps</code>	0.15
	<code>min_samples</code>	16
C-DBSCAN	<code>eps</code>	0.24
	<code>min_pts</code>	16

6. <https://github.com/LorenzoMonti/RRLs-Clustering-Benchmark>

References

Tiba Zaki Abdulhameed, Suhad A Yousif, Venus W Samawi, and Hasnaa Imad Al-Shaikhli. Ss-dbscan: Semi-supervised density-based spatial clustering of applications with noise for meaningful clustering in diverse density data. *IEEE Access*, 12:131507–131520, 2024.

Mihael Ankerst, Markus M Breunig, Hans-Peter Kriegel, and Jörg Sander. Optics: Ordering points to identify the clustering structure. *ACM Sigmod record*, 28(2):49–60, 1999.

M Baghshah and S Shouraki. Kernel-based metric learning for semi-supervised clustering. *Neurocomputing*, 2010. Based on Source 212.

Sugato Basu and Raymond Mooney. Semi-supervised clustering: Probabilistic models, algorithms and experiments. *Proceedings of the 22nd international conference on machine learning*, 2005. Based on Source 225.

Sugato Basu, Arindam Banerjee, and Raymond J Mooney. Semi-supervised clustering by seeding. In *Proceedings of the nineteenth international conference on machine learning*, pages 27–34, 2002.

Sugato Basu, Arindam Banerjee, and Raymond J Mooney. Active semi-supervision for pairwise constrained clustering. In *Proceedings of the 2004 SIAM international conference on data mining*, pages 333–344. SIAM, 2004a.

Sugato Basu, Mikhail Bilenko, and Raymond J Mooney. A probabilistic framework for semi-supervised clustering. In *Proceedings of the tenth ACM SIGKDD international conference on Knowledge discovery and data mining*, 2004b. Based on Source 224.

P Baumann and D Hochbaum. An algorithm for clustering with confidence-based must-link and cannot-link constraints. *INFORMS Journal on Computing*, 2022. Based on Source 216.

V. Belokurov, D. Erkal, N. W. Evans, S. E. Koposov, and A. J. Deason. Co-formation of the disc and the stellar halo. *Monthly Notices of the Royal Astronomical Society*, 478(1): 611–619, July 2018. doi: 10.1093/mnras/sty982.

G. Bono, F. Caputo, V. Castellani, M. Marconi, J. Storm, and S. Degl’Innocenti. A pulsational approach to near-infrared and visual magnitudes of RR Lyr stars. *Monthly Notices of the Royal Astronomical Society*, 344(4):1097–1106, October 2003. doi: 10.1046/j.1365-8711.2003.06878.x.

Jianghui Cai, Jing Hao, Haifeng Yang, Xujun Zhao, and Yuqing Yang. A review on semi-supervised clustering. *Information Sciences*, 632:164–200, 2023.

Ricardo JGB Campello, Davoud Moulavi, and Jörg Sander. Density-based clustering based on hierarchical density estimates. In *Pacific-Asia conference on knowledge discovery and data mining*, pages 160–172. Springer, 2013.

Ricardo JGB Campello, Davoud Moulavi, Arthur Zimek, and Jörg Sander. Hierarchical density estimates for data clustering, visualization, and outlier detection. *ACM Transactions on Knowledge Discovery from Data (TKDD)*, 10(1):1–51, 2015.

E Ceccarelli, D Massari, A Mucciarelli, M Bellazzini, A Nunnari, F Cusano, C Lardo, D Romano, I Ilyin, and A Stokholm. A walk on the retrograde side (wrs) project-i. tidying-up the retrograde halo with high-resolution spectroscopy. *Astronomy & Astrophysics*, 684: A37, 2024.

Gisella Clementini, Raffaele Gratton, Angela Bragaglia, Eugenio Carretta, Luca Di Fabrizio, and Marcella Maio. Distance to the Large Magellanic Cloud: The RR Lyrae Stars. *Astron. J.*, 125(3):1309–1329, March 2003. doi: 10.1086/367773.

Ian Davidson and SS Ravi. Agglomerative hierarchical clustering with constraints: Theoretical and empirical results. In *European Conference on Principles of Data Mining and Knowledge Discovery*, pages 59–70. Springer, 2005.

David L Davies and Donald W Bouldin. A cluster separation measure. *IEEE transactions on pattern analysis and machine intelligence*, PAMI-1(2):224–227, 2009.

Emma Dodd, Thomas M. Callingham, Amina Helmi, Tadafumi Matsuno, Tomás Ruiz-Lara, Eduardo Balbinot, and Sofie Lövdal. Gaia DR3 view of dynamical substructure in the stellar halo near the Sun. *Astron. Astrophys.*, 670:L2, February 2023. doi: 10.1051/0004-6361/202244546.

Martin Ester, Hans-Peter Kriegel, Jörg Sander, Xiaowei Xu, et al. A density-based algorithm for discovering clusters in large spatial databases with noise. In *kdd*, volume 96, pages 226–231, 1996.

Gaia Collaboration, T. Prusti, J. H. J. de Bruijne, A. G. A. Brown, A. Vallenari, C. Babusiaux, C. A. L. Bailer-Jones, U. Bastian, M. Biermann, D. W. Evans, L. Eyer, F. Jansen, C. Jordi, S. A. Klioner, U. Lammers, L. Lindegren, X. Luri, F. Mignard, D. J. Milligan, C. Panem, V. Poinsignon, D. Pourbaix, S. Randich, G. Sarri, P. Sartoretti, H. I. Siddiqui, C. Soubiran, V. Valette, F. van Leeuwen, N. A. Walton, C. Aerts, F. Arenou, M. Cropper, R. Drimmel, E. Høg, D. Katz, M. G. Lattanzi, W. O’Mullane, E. K. Grebel, A. D. Holland, C. Huc, X. Passot, L. Bramante, C. Cacciari, J. Castañeda, L. Chaoul, N. Cheek, F. De Angeli, C. Fabricius, R. Guerra, J. Hernández, A. Jean-Antoine-Piccolo, E. Masana, R. Messineo, N. Mowlavi, K. Nienartowicz, D. Ordóñez-Blanco, P. Panuzzo, J. Portell, P. J. Richards, M. Riello, G. M. Seabroke, P. Tanga, F. Thévenin, J. Torra, S. G. Els, G. Gracia-Abril, G. Comoretto, M. Garcia-Reinaldos, T. Lock, E. Mercier, M. Altmann, R. Andrae, T. L. Astraatmadja, I. Bellas-Velidis, K. Benson, J. Berthier, R. Blomme, G. Busso, B. Carry, A. Cellino, G. Clementini, S. Cowell, O. Creevey, J. Cuypers, M. Davidson, J. De Ridder, A. de Torres, L. Delchambre, A. Dell’Oro, C. Ducourant, Y. Frémat, M. García-Torres, E. Gosset, J. L. Halbwachs, N. C. Hambly, D. L. Harrison, M. Hauser, D. Hestroffer, S. T. Hodgkin, H. E. Huckle, A. Hutton, G. Jasniewicz, S. Jordan, M. Kontizas, A. J. Korn, A. C. Lanzafame, M. Manteiga, A. Moitinho, K. Muinonen, J. Osinde, E. Pancino, T. Pauwels, J. M. Petit, A. Recio-Blanco, A. C. Robin, L. M. Sarro, C. Siopis, M. Smith, K. W. Smith, A. Sozzetti, W. Thuillot, W. van Reeven, Y. Viala, U. Abbas, A. Abreu Aramburu, S. Accart, J. J. Aguado, P. M. Allan, W. Alasia, G. Altavilla, M. A. Álvarez, J. Alves, R. I. Anderson, A. H. Andrei, E. Anglada Varela, E. Antiche, T. Antoja, S. Antón, B. Arcay, A. Atzei, L. Ayache, N. Bach, S. G.

Baker, L. Balaguer-Núñez, C. Barache, C. Barata, A. Barbier, F. Barblan, M. Baroni, D. Barrado y Navascués, M. Barros, M. A. Barstow, U. Becciani, M. Bellazzini, G. Bellei, A. Bello García, V. Belokurov, P. Bendjoya, A. Berihuete, L. Bianchi, O. Bienaymé, F. Billebaud, N. Blagorodnova, S. Blanco-Cuaresma, T. Boch, A. Bombrun, R. Borrachero, S. Bouquillon, G. Bourda, H. Bouy, A. Bragaglia, M. A. Breddels, N. Brouillet, T. Brüsemeister, B. Bucciarelli, F. Budnik, P. Burgess, R. Burgon, A. Burlacu, D. Busonero, R. Buzzi, E. Caffau, J. Cambras, H. Campbell, R. Cancelliere, T. Cantat-Gaudin, T. Carlucci, J. M. Carrasco, M. Castellani, P. Charlot, J. Charnas, P. Charvet, F. Chassat, A. Chiavassa, M. Clotet, G. Cocozza, R. S. Collins, P. Collins, G. Costigan, F. Crifo, N. J. G. Cross, M. Crosta, C. Crowley, C. Dafonte, Y. Damerdji, A. Dapergolas, P. David, M. David, P. De Cat, F. de Felice, P. de Laverny, F. De Luise, R. De March, D. de Martino, R. de Souza, J. Debosscher, E. del Pozo, M. Delbo, A. Delgado, H. E. Delgado, F. di Marco, P. Di Matteo, S. Diakite, E. Distefano, C. Dolding, S. Dos Anjos, P. Drazinos, J. Durán, Y. Dzigan, E. Ecale, B. Edvardsson, H. Enke, M. Erdmann, D. Escolar, M. Espina, N. W. Evans, G. Eynard Bontemps, C. Fabre, M. Fabrizio, S. Faigler, A. J. Falcão, M. Farràs Casas, F. Faye, L. Federici, G. Fedorets, J. Fernández-Hernández, P. Fernique, A. Fienga, F. Figueras, F. Filippi, K. Findeisen, A. Fonti, M. Fouesneau, E. Fraile, M. Fraser, J. Fuchs, R. Furnell, M. Gai, S. Galleti, L. Galluccio, D. Garabato, F. García-Sedano, P. Garé, A. Garofalo, N. Garralda, P. Gavras, J. Gerssen, R. Geyer, G. Gilmore, S. Girona, G. Giuffrida, M. Gomes, A. González-Marcos, J. González-Núñez, J. J. González-Vidal, M. Granvik, A. Guerrier, P. Guillout, J. Guiraud, A. Gúrpide, R. Gutiérrez-Sánchez, L. P. Guy, R. Haigron, D. Hatzidimitriou, M. Haywood, U. Heiter, A. Helmi, D. Hobbs, W. Hofmann, B. Holl, G. Holland, J. A. S. Hunt, A. Hypki, V. Icardi, M. Irwin, G. Jevardat de Fombelle, P. Jofré, P. G. Jonker, A. Jorissen, F. Julbe, A. Karampelas, A. Kochoska, R. Kohley, K. Kolenberg, E. Kontizas, S. E. Koposov, G. Kordopatis, P. Koubsky, A. Kowalczyk, A. Krone-Martins, M. Kudryashova, I. Kull, R. K. Bachchan, F. Lacoste-Seris, A. F. Lanza, J. B. Lavigne, C. Le Poncin-Lafitte, Y. Lebreton, T. Lebzelter, S. Leccia, N. Leclerc, I. Lecoeur-Taibi, V. Lemaitre, H. Lenhardt, F. Leroux, S. Liao, E. Licata, H. E. P. Lindstrøm, T. A. Lister, E. Livanou, A. Lobel, W. Löffler, M. López, A. Lopez-Lozano, D. Lorenz, T. Loureiro, I. MacDonald, T. Magalhães Fernandes, S. Managau, R. G. Mann, G. Mantelet, O. Marchal, J. M. Marchant, M. Marconi, J. Marie, S. Marinoni, P. M. Marrese, G. Marschalkó, D. J. Marshall, J. M. Martín-Fleitas, M. Martino, N. Mary, G. Matijević, T. Mazeh, P. J. McMillan, S. Messina, A. Mestre, D. Michalik, N. R. Millar, B. M. H. Miranda, D. Molina, R. Molinaro, M. Molinaro, L. Molnár, M. Moniez, P. Montegriffo, D. Monteiro, R. Mor, A. Mora, R. Morbidelli, T. Morel, S. Morgenthaler, T. Morley, D. Morris, A. F. Mulone, T. Muraveva, I. Musella, J. Narbonne, G. Nelemans, L. Nicastro, L. Noval, C. Ordénovic, J. Ordieres-Meré, P. Osborne, C. Pagani, I. Pagano, F. Pailler, H. Palacin, L. Palaversa, P. Parsons, T. Paulsen, M. Pecoraro, R. Pedrosa, H. Pentikäinen, J. Pereira, B. Pichon, A. M. Piersimoni, F. X. Pineau, E. Plachy, G. Plum, E. Poujoulet, A. Prša, L. Pulone, S. Ragaini, S. Rago, N. Rambaux, M. Ramos-Lerate, P. Ranalli, G. Rauw, A. Read, S. Regibo, F. Renk, C. Reylé, R. A. Ribeiro, L. Rimoldini, V. Ripepi, A. Riva, G. Rixon, M. Roelens, M. Romero-Gómez, N. Rowell, F. Royer, A. Rudolph, L. Ruiz-Dern, G. Sadowski, T. Sagristà Sellés, J. Sahlmann, J. Salgado, E. Salguero, M. Sarasso, H. Savietto, A. Schnorhk, M. Schultheis, E. Sciacca, M. Segol, J. C. Segovia, D. Segransan, E. Serpell,

I. C. Shih, R. Smareglia, R. L. Smart, C. Smith, E. Solano, F. Solitro, R. Sordo, S. Soria Nieto, J. Souchay, A. Spagna, F. Spoto, U. Stampa, I. A. Steele, H. Steidelmüller, C. A. Stephenson, H. Stoev, F. F. Suess, M. Süveges, J. Surdej, L. Szabados, E. Szegedi-Elek, D. Tapiador, F. Taris, G. Tauran, M. B. Taylor, R. Teixeira, D. Terrett, B. Tingley, S. C. Trager, C. Turon, A. Ulla, E. Utrilla, G. Valentini, A. van Elteren, E. Van Hemelryck, M. van Leeuwen, M. Varadi, A. Vecchiato, J. Veljanoski, T. Via, D. Vicente, S. Vogt, H. Voss, V. Votruba, S. Voutsinas, G. Walmsley, M. Weiler, K. Weingrill, D. Werner, T. Wevers, G. Whitehead, L. Wyrzykowski, A. Yoldas, M. Žerjal, S. Zucker, C. Zurbach, T. Zwitter, A. Alecu, M. Allen, C. Allende Prieto, A. Amorim, G. Anglada-Escudé, V. Arsenijevic, S. Azaz, P. Balm, M. Beck, H. H. Bernstein, L. Bigot, A. Bijaoui, C. Blasco, M. Bonfigli, G. Bono, S. Boudreault, A. Bressan, S. Brown, P. M. Brunet, P. Bunclark, R. Buonanno, A. G. Butkevich, C. Carret, C. Carrion, L. Chemin, F. Chéreau, L. Corcione, E. Darmigny, K. S. de Boer, P. de Teodoro, P. T. de Zeeuw, C. Delle Luche, C. D. Domingues, P. Dubath, F. Fodor, B. Frézouls, A. Fries, D. Fustes, D. Fyfe, E. Gallardo, J. Gallegos, D. Gardiol, M. Gebran, A. Gomboc, A. Gómez, E. Grux, A. Gueguen, A. Heyrovsky, J. Hoar, G. Iannicola, Y. Isasi Parache, A. M. Janotto, E. Joliet, A. Jonckheere, R. Keil, D. W. Kim, P. Klagyivik, J. Klar, J. Knude, O. Kochukhov, I. Kolka, J. Kos, A. Kutka, V. Lainey, D. LeBouquin, C. Liu, D. Loreggia, V. V. Makarov, M. G. Marseille, C. Martayan, O. Martinez-Rubi, B. Massart, F. Meynadier, S. Mignot, U. Munari, A. T. Nguyen, T. Nordlander, P. Ocvirk, K. S. O'Flaherty, A. Olias Sanz, P. Ortiz, J. Osorio, D. Oszkiewicz, A. Ouzounis, M. Palmer, P. Park, E. Pasquato, C. Peltzer, J. Peralta, F. Pétruraud, T. Pieniluoma, E. Pigozzi, J. Poels, G. Prat, T. Prod'homme, F. Raison, J. M. Rebordao, D. Risquez, B. Rocca-Volmerange, S. Rosen, M. I. Ruiz-Fuertes, F. Russo, S. Sembay, I. Serraller Vizcaino, A. Short, A. Siebert, H. Silva, D. Sinachopoulos, E. Slezak, M. Soffel, D. Sosnowska, V. Straižys, M. ter Linden, D. Terrell, S. Theil, C. Tiede, L. Troisi, P. Tsalmantza, D. Tur, M. Vaccari, F. Vachier, P. Valles, W. Van Hamme, L. Veltz, J. Virtanen, J. M. Wallut, R. Wichmann, M. I. Wilkinson, H. Ziaeepour, and S. Zschocke. The Gaia mission. *Astron. Astrophys.*, 595:A1, November 2016. doi: 10.1051/0004-6361/201629272.

Gaia Collaboration, A. Vallenari, A. G. A. Brown, T. Prusti, J. H. J. de Bruijne, F. Arenou, C. Babusiaux, M. Biermann, O. L. Creevey, C. Ducourant, D. W. Evans, L. Eyer, R. Guerra, A. Hutton, C. Jordi, S. A. Klioner, U. L. Lammers, L. Lindegren, X. Luri, F. Mignard, C. Panem, D. Pourbaix, S. Randich, P. Sartoretti, C. Soubiran, P. Tanga, N. A. Walton, C. A. L. Bailer-Jones, U. Bastian, R. Drimmel, F. Jansen, D. Katz, M. G. Lattanzi, F. van Leeuwen, J. Bakker, C. Cacciari, J. Castañeda, F. De Angeli, C. Fabricius, M. Fouesneau, Y. Frémat, L. Galluccio, A. Guerrier, U. Heiter, E. Masana, R. Messineo, N. Mowlavi, C. Nicolas, K. Nienartowicz, F. Pailler, P. Panuzzo, F. Riclet, W. Roux, G. M. Seabroke, R. Sordo, F. Thévenin, G. Gracia-Abril, J. Portell, D. Teyssier, M. Altmann, R. Andrae, M. Audard, I. Bellas-Velidis, K. Benson, J. Berthier, R. Blomme, P. W. Burgess, D. Busonero, G. Busso, H. Cánovas, B. Carry, A. Cellino, N. Cheek, G. Clementini, Y. Damerdji, M. Davidson, P. de Teodoro, M. Nuñez Campos, L. Delchambre, A. Dell'Oro, P. Esquej, J. Fernández-Hernández, E. Fraile, D. Garabato, P. García-Lario, E. Gosset, R. Haigron, J. L. Halbwachs, N. C. Hambly, D. L. Harrison, J. Hernández, D. Hestroffer, S. T. Hodgkin, B. Holl, K. Janßen, G. Jevardat de Fombelle, S. Jordan,

A. Krone-Martins, A. C. Lanzafame, W. Löffler, O. Marchal, P. M. Marrese, A. Moitinho, K. Muinonen, P. Osborne, E. Pancino, T. Pauwels, A. Recio-Blanco, C. Reylé, M. Riello, L. Rimoldini, T. Roegiers, J. Rybizki, L. M. Sarro, C. Siopsis, M. Smith, A. Sozzetti, E. Utrilla, M. van Leeuwen, U. Abbas, P. Ábrahám, A. Abreu Aramburu, C. Aerts, J. J. Aguado, M. Ajaj, F. Aldea-Montero, G. Altavilla, M. A. Álvarez, J. Alves, F. Anders, R. I. Anderson, E. Anglada Varela, T. Antoja, D. Baines, S. G. Baker, L. Balaguer-Núñez, E. Balbinot, Z. Balog, C. Barache, D. Barbato, M. Barros, M. A. Barstow, S. Bartolomé, J. L. Bassilana, N. Bauchet, U. Becciani, M. Bellazzini, A. Berihuete, M. Berne, S. Bertone, L. Bianchi, A. Binnenfeld, S. Blanco-Cuaresma, A. Blazere, T. Boch, A. Bombrun, D. Bossini, S. Bouquillon, A. Bragaglia, L. Bramante, E. Breedt, A. Bresan, N. Brouillet, E. Brugaletta, B. Bucciarelli, A. Burlacu, A. G. Butkevich, R. Buzzi, E. Caffau, R. Cancelliere, T. Cantat-Gaudin, R. Carballo, T. Carlucci, M. I. Carnerero, J. M. Carrasco, L. Casamiquela, M. Castellani, A. Castro-Ginard, L. Chaoul, P. Charlot, L. Chemin, V. Chiaramida, A. Chiavassa, N. Chornay, G. Comoretto, G. Contursi, W. J. Cooper, T. Cornez, S. Cowell, F. Crifo, M. Cropper, M. Crosta, C. Crowley, C. Dafonte, A. Dapergolas, M. David, P. David, P. de Laverny, F. De Luise, R. De March, J. De Ridder, R. de Souza, A. de Torres, E. F. del Peloso, E. del Pozo, M. Delbo, A. Delgado, J. B. Delisle, C. Demouchy, T. E. Dharmawardena, P. Di Matteo, S. Diakite, C. Diener, E. Distefano, C. Dolding, B. Edvardsson, H. Enke, C. Fabre, M. Fabrizio, S. Faigler, G. Fedorets, P. Fernique, A. Fienga, F. Figueiras, Y. Fournier, C. Fouron, F. Frakoudi, M. Gai, A. Garcia-Gutierrez, M. Garcia-Reinaldos, M. García-Torres, A. Garofalo, A. Gavel, P. Gavras, E. Gerlach, R. Geyer, P. Giacobbe, G. Gilmore, S. Girona, G. Giuffrida, R. Gomel, A. Gomez, J. González-Núñez, I. González-Santamaría, J. J. González-Vidal, M. Granvik, P. Guillout, J. Guiraud, R. Gutiérrez-Sánchez, L. P. Guy, D. Hatzidimitriou, M. Hauser, M. Haywood, A. Helmer, A. Helmi, M. H. Sarmiento, S. L. Hidalgo, T. Hilger, N. Hładcuk, D. Hobbs, G. Holland, H. E. Huckle, K. Jardine, G. Jasniewicz, A. Jean-Antoine Piccolo, Ó. Jiménez-Arranz, A. Jorissen, J. Juaristi Campillo, F. Julbe, L. Karbevska, P. Kervella, S. Khanna, M. Kontizas, G. Kordopatis, A. J. Korn, Á. Kóspál, Z. Kostrzewska-Rutkowska, K. Kruszyńska, M. Kun, P. Laizeau, S. Lambert, A. F. Lanza, Y. Lasne, J. F. Le Campion, Y. Lebreton, T. Lebzelter, S. Leccia, N. Leclerc, I. Lecoeur-Taibi, S. Liao, E. L. Licata, H. E. P. Lindström, T. A. Lister, E. Livanou, A. Lobel, A. Lorca, C. Loup, P. Madrero Pardo, A. Magdaleno Romeo, S. Managau, R. G. Mann, M. Manteiga, J. M. Marchant, M. Marconi, J. Marcos, M. M. S. Marcos Santos, D. Marín Pina, S. Marinoni, F. Marocco, D. J. Marshall, L. Martin Polo, J. M. Martín-Fleitas, G. Marton, N. Mary, A. Masip, D. Massari, A. Mastrobuono-Battisti, T. Mazeh, P. J. McMillan, S. Messina, D. Michalik, N. R. Millar, A. Mints, D. Molina, R. Molinaro, L. Molnár, G. Monari, M. Monguió, P. Montegriffo, A. Montero, R. Mor, A. Mora, R. Morbidelli, T. Morel, D. Morris, T. Muraveva, C. P. Murphy, I. Musella, Z. Nagy, L. Noval, F. Ocaña, A. Ogden, C. Ordenovic, J. O. Osinde, C. Pagani, I. Pagano, L. Palaversa, P. A. Palicio, L. Pallas-Quintela, A. Panahi, S. Payne-Wardenaar, X. Peñalosa Esteller, A. Penttilä, B. Pichon, A. M. Piersimoni, F. X. Pineau, E. Plachy, G. Plum, E. Poggio, A. Prša, L. Pulone, E. Racero, S. Ragaini, M. Rainer, C. M. Raiteri, N. Rambaux, P. Ramos, M. Ramos-Lerate, P. Re Fiorentin, S. Regibo, P. J. Richards, C. Rios Diaz, V. Ripepi, A. Riva, H. W. Rix, G. Rixon, N. Robichon, A. C. Robin, C. Robin, M. Roelens, H. R. O. Rogues, L. Rohrbasser, M. Romero-Gómez, N. Rowell, F. Royer, D. Ruz Mieres,

K. A. Rybicki, G. Sadowski, A. Sáez Núñez, A. Sagristà Sellés, J. Sahlmann, E. Salguero, N. Samaras, V. Sanchez Gimenez, N. Sanna, R. Santoveña, M. Sarasso, M. Schultheis, E. Sciacca, M. Segol, J. C. Segovia, D. Ségransan, D. Semeux, S. Shahaf, H. I. Siddiqui, A. Siebert, L. Siltala, A. Silvelo, E. Slezak, I. Slezak, R. L. Smart, O. N. Snaith, E. Solano, F. Solitro, D. Souami, J. Souchay, A. Spagna, L. Spina, F. Spoto, I. A. Steele, H. Steidelmüller, C. A. Stephenson, M. Süveges, J. Surdej, L. Szabados, E. Szegedi-Elek, F. Taris, M. B. Taylor, R. Teixeira, L. Tolomei, N. Tonello, F. Torra, J. Torra, G. Torralba Elipe, M. Trabucchi, A. T. Tsounis, C. Turon, A. Ulla, N. Unger, M. V. Vaillant, E. van Dillen, W. van Reeven, O. Vanel, A. Vecchiato, Y. Viala, D. Vicente, S. Voutsinas, M. Weiler, T. Wevers, L. Wyrzykowski, A. Yoldas, P. Yvard, H. Zhao, J. Zorec, S. Zucker, and T. Zwitter. Gaia Data Release 3. Summary of the content and survey properties. *Astron. Astrophys.*, 674:A1, June 2023. doi: 10.1051/0004-6361/202243940.

Haitao Gan, Yingle Fan, Zhizeng Luo, Rui Huang, and Zhi Yang. Confidence-weighted safe semi-supervised clustering. *Engineering Applications of Artificial Intelligence*, 81: 107–116, 2019.

Germán González-Almagro, Daniel Peralta, ED Poorter, J Cano, and Salvador García. Semi-supervised constrained clustering: An in-depth overview, ranked taxonomy and future research directions. *arXiv preprint arXiv:2301.xxxxx*, 2023. Based on Source 205.

Nizar Grira, Michel Crucianu, and Nozha Boujemaa. Active semi-supervised fuzzy clustering. *Pattern Recognition*, 41(5):1834–1844, 2008.

Jun Gu, Wei Feng, Jia Zeng, Hiroshi Mamitsuka, and Shanfeng Zhu. Efficient semisupervised medline document clustering with mesh-semantic and global-content constraints. *IEEE Transactions on Cybernetics*, 2013. Based on Source 209.

Amina Helmi. Streams, substructures, and the early history of the milky way. *Annual Review of Astronomy and Astrophysics*, 58(1):205–256, 2020.

Amina Helmi and P Tim de Zeeuw. Mapping the substructure in the galactic halo with the next generation of astrometric satellites. *Monthly Notices of the Royal Astronomical Society*, 319(3):657–665, 2000.

Amina Helmi, Carine Babusiaux, Helmer H. Koppelman, Davide Massari, Jovan Veljanoski, and Anthony G. A. Brown. The merger that led to the formation of the Milky Way’s inner stellar halo and thick disk. *Nature*, 563(7729):85–88, October 2018. doi: 10.1038/s41586-018-0625-x.

Lawrence Hubert and Phipps Arabie. Comparing partitions. *Journal of classification*, 2(1): 193–218, 1985.

D Ienco and R Interdonato. Deep semi-supervised clustering for multi-variate time-series. *Neurocomputing*, 2022. Based on Source 203.

D Ienco and R Pensa. Semi-supervised clustering with multiresolution autoencoders. In *IEEE International Joint Conference on Neural Networks (IJCNN)*, 2018. Based on Source 204.

He Jiang, Zhilei Ren, J Xuan, and Xindong Wu. Extracting elite pairwise constraints for clustering. *Neurocomputing*, 2013. Based on Source 208.

J. Jurcsik and G. Kovacs. Determination of [Fe/H] from the light curves of RR Lyrae stars. *Astron. Astrophys.*, 312:111–120, August 1996.

A. J. Longmore, J. A. Fernley, and R. F. Jameson. RR Lyrae stars in globular clusters : better distances from infrared measurements ? *Monthly Notices of the Royal Astronomical Society*, 220:279–287, May 1986. doi: 10.1093/mnras/220.2.279.

Khyati Malhan and Hans-Walter Rix. Shiva and Shakti: Presumed Proto-Galactic Fragments in the Inner Milky Way. *Astrophys. J.*, 964(2):104, April 2024. doi: 10.3847/1538-4357/ad1885.

Davide Massari, Helmer H Koppelman, and Amina Helmi. Origin of the system of globular clusters in the milky way. *Astronomy & Astrophysics*, 630:L4, 2019.

Tadafumi Matsuno, Wako Aoki, and Takuma Suda. Origin of the Excess of High-energy Retrograde Stars in the Galactic Halo. *Astrophys. J. Lett.*, 874(2):L35, April 2019. doi: 10.3847/2041-8213/ab0ec0.

James B McQueen. Some methods of classification and analysis of multivariate observations. In *Proc. of 5th Berkeley Symposium on Math. Stat. and Prob.*, pages 281–297, 1967.

Siobahn M. Morgan, Jennifer N. Wahl, and Rachel M. Wieckhorst. [Fe/H] relations for c-type RR Lyrae variables based upon Fourier coefficients. *Monthly Notices of the Royal Astronomical Society*, 374(4):1421–1426, February 2007. doi: 10.1111/j.1365-2966.2006.11247.x.

Tatiana Muraveva, Hector E. Delgado, Gisella Clementini, Luis M. Sarro, and Alessia Garofalo. RR Lyrae stars as standard candles in the Gaia Data Release 2 Era. *Monthly Notices of the Royal Astronomical Society*, 481(1):1195–1211, November 2018. doi: 10.1093/mnras/sty2241.

Tatiana Muraveva, Andrea Giannetti, Gisella Clementini, Alessia Garofalo, and Lorenzo Monti. Metallicity of RR Lyrae stars from the Gaia Data Release 3 catalogue computed with Machine Learning algorithms. *Monthly Notices of the Royal Astronomical Society*, 536(3):2749–2769, January 2025. doi: 10.1093/mnras/stae2679.

G. C. Myeong, E. Vasiliev, G. Iorio, N. W. Evans, and V. Belokurov. Evidence for two early accretion events that built the Milky Way stellar halo. *Monthly Notices of the Royal Astronomical Society*, 488(1):1235–1247, September 2019. doi: 10.1093/mnras/stz1770.

Yue Qin, Shifei Ding, Lijuan Wang, and Yanru Wang. Research progress on semi-supervised clustering. *Cognitive Computation*, 11(5):599–612, 2019.

Yazhou Ren, Kangrong Hu, Xinyi Dai, Lili Pan, Steven CH Hoi, and Zenglin Xu. Semi-supervised deep embedded clustering. *Neurocomputing*, 325:121–130, 2019.

Andrew Rosenberg and Julia Hirschberg. V-measure: A conditional entropy-based external cluster evaluation measure. In *Proceedings of the 2007 joint conference on empirical methods in natural language processing and computational natural language learning (EMNLP-CoNLL)*, pages 410–420, 2007.

Carlos Ruiz, Myra Spiliopoulou, and Ernestina Menasalvas. C-dbscan: Density-based clustering with constraints. In *International workshop on rough sets, fuzzy sets, data mining, and granular-soft computing*, pages 216–223. Springer, 2007.

Amit Salunke, Xumin Liu, and M Rege. Constrained co-clustering with non-negative matrix factorisation. *International Journal of Business Intelligence and Data Mining*, 2012. Based on Source 198.

Marek Śmieja, Lukasz Struski, and Mário AT Figueiredo. A classification-based approach to semi-supervised clustering with pairwise constraints. *Neural Networks*, 2020. Based on Source 214.

A. Sollima, C. Cacciari, A. A. H. Arkharov, V. M. Larionov, D. L. Gorshanov, N. V. Efimova, and A. Piersimoni. The infrared JHK light curves of RR Lyr. *Monthly Notices of the Royal Astronomical Society*, 384(4):1583–1587, March 2008. doi: 10.1111/j.1365-2966.2007.12804.x.

Guillaume Wacquet, Émilie Poisson-Caillault, and Pierre-Alexandre Hébert. Semi-supervised k-way spectral clustering with determination of number of clusters. In *International Joint Conference on Computational Intelligence*, pages 317–332. Springer, 2011.

Kiri Wagstaff, Claire Cardie, Seth Rogers, Stefan Schrödl, et al. Constrained k-means clustering with background knowledge. In *Icml*, volume 1, pages 577–584, 2001.

Eric Xing, Michael Jordan, Stuart J Russell, and Andrew Ng. Distance metric learning with application to clustering with side-information. *Advances in neural information processing systems*, 15, 2002.

Sicheng Xiong, J Azimi, and Xiaoli Z Fern. Active learning of constraints for semi-supervised clustering. *IEEE Transactions on Knowledge and Data Engineering*, 2014. Based on Source 222.

Yan Yang, Wei Tan, Tianrui Li, and Da Ruan. Consensus clustering based on constrained self-organizing map and improved cop-kmeans ensemble in intelligent decision support systems. *Knowledge-Based Systems*, 32:101–115, 2012.

Yun Yang, Zongze Li, Wei Wang, and Dapeng Tao. An adaptive semi-supervised clustering approach via multiple density-based information. *Neurocomputing*, 257:193–205, 2017.

Jieping Ye, Zheng Zhao, and Huan Liu. Adaptive distance metric learning for clustering. In *2007 IEEE Conference on Computer Vision and Pattern Recognition*, pages 1–7. IEEE, 2007.

Hong Zhang, Jun Yu, Meng Wang, and Yun Liu. Semi-supervised distance metric learning based on local linear regression for data clustering. *Neurocomputing*, 93:100–105, 2012.